

## Role of the quasifission yields in the multinucleon transfer reactions of $^{136}\text{Xe} + ^{208}\text{Pb}$

Gen Zhang,<sup>1,2</sup> Jing-Jing Li,<sup>1,2</sup> Xin-Rui Zhang,<sup>1,2</sup> Bing Li,<sup>1,2</sup> Cheikh A. T. Sokhna,<sup>1,2</sup> Chen Wang,<sup>1,2</sup> Zhong Liu,<sup>3,4</sup> and Feng-Shou Zhang<sup>1,2,5,\*</sup>

<sup>1</sup>The Key Laboratory of Beam Technology of Ministry of Education, College of Nuclear Science and Technology, Beijing Normal University, Beijing 100875, China

<sup>2</sup>Beijing Radiation Center, Beijing 100875, China

<sup>3</sup>CAS Key Laboratory of High Precision Nuclear Spectroscopy, Institute of Modern Physics, Lanzhou 730000, China

<sup>4</sup>School of Nuclear Science and Technology, University of Chinese Academy of Sciences, Beijing, 100049 China

<sup>5</sup>Center of Theoretical Nuclear Physics, National Laboratory of Heavy Ion Accelerator of Lanzhou, Lanzhou 730000, China



(Received 4 June 2020; accepted 27 July 2020; published 14 August 2020)

The mass distribution in  $^{136}\text{Xe} + ^{208}\text{Pb}$  is investigated within the dinuclear system model. With the contribution of quasifission yields, the probability of all the fragments is conserved, and the mass distribution becomes wider with increasing the evolution time. The difference between including and excluding the contribution of quasifission yields is more obvious at a lower angular momentum. The cross sections, including quasifission yields in the region with mass less than the projectile and more than the target, are closer to the experimental data. The impact from the quasifission yields on the neutron-deficient isotopes is greater than the neutron-rich ones. The quasifission yields concentrate on the initial stage of evolution time, corresponding to a lower excitation energy. Considering the time-dependent excitation energy of the quasifission fragments produced within the interaction time, fewer neutrons are evaporated comparing to the case with the excitation energy at the interaction time.

DOI: [10.1103/PhysRevC.102.024617](https://doi.org/10.1103/PhysRevC.102.024617)

### I. INTRODUCTION

The quasifission phenomena in heavy-ion collisions were discovered in the reaction  $^{132}\text{Xe} + ^{56}\text{Fe}$  in the late 1970s, demonstrating it as a new type of strongly damped collision at that time [1]. Quasifission is a fissionlike process, and it is rather difficult to distinguish the quasifission and fusion-fission in the experiments [2]. In terms of mass division and reaction time scales, the quasifission provides a bridge between the deep inelastic scattering process and the complete fusion process. In deep inelastic scattering, the memory of the entrance channel like the mass-asymmetry is preserved [3,4]. However, the compound nuclei formed in the complete fusion process lose the memory of projectile and target, conserving only global properties. Quasifission is characterized by a massive mass drift away from the initial mass asymmetry in the entrance channel [5].

In the experiments with a  $^{208}\text{Pb}$  beam performed at GSI, an enhanced width of the symmetric mass distribution and the anisotropy of symmetric fragments were observed, which can be explained as the effect of quasifission [6]. The quasifission products range from initial entrance-channel mass asymmetry all the way to symmetry, and the amount of mass drift takes on any value depending on the incident energy, the orbital angular momentum, and the charge numbers of the interacting nuclei [5,7–11]. At high angular momenta, the fissionlike

fragments are mainly attributed to the quasifission [12]. The relaxation of angular momentum in quasifission reactions was terminated before full statistical spin equilibrium was reached [13].

The mass asymmetry of the entrance channel plays an important role in the nucleon flow in quasifission process [14–16]. By measuring the fission fragment mass-angle correlations and width of mass distribution, it was observed that the quasifission is more significant in the more mass-symmetric reactions [17,18]. For example, the measured width of mass distribution in  $^{18}\text{O} + ^{232}\text{Th}$  reaction is larger than  $^{12}\text{C} + ^{238}\text{U}$ , indicating the quasifission is more evident in the former [18]. In the collisions with projectiles heavier than  $A = 20$ , quasifission processes lead to a different distribution of  $K$  values from that predicted by the standard theory [19]. The influence of nuclear orientation on quasifission is also analyzed. In  $^{16}\text{O} + ^{238}\text{U}$  reaction, it was found that collisions with the tips of  $^{238}\text{U}$  target would predominantly lead to quasifission, while the collisions with the sides of the target would mainly cause fusion-fission [20,21].

For the fusion reactions, the quasifission processes suppress the complete fusion of heavy ions [22–25]. Nevertheless, in the asymmetry-exit-channel (i.e., the exit channel with mass asymmetry larger than one in the entrance channel) quasifission reactions using actinide targets, the superheavy nuclei can be produced [26–28].

Several models are developed to describe the quasifission processes [22,29–35]. A fully microscopic time-dependent

\*Corresponding author: fszhang@bnu.edu.cn

Hartree-Fock (TDHF) model is applied to investigate the dissipative dynamics in quasifission reactions [32–43]. It is found that the quasifission is much reduced with  $^{48}\text{Ca}$  projectile than the  $^{40}\text{Ca}$  case, which explains the advantages of using  $^{48}\text{Ca}$  to synthesize superheavy elements [35]. The timescales of equilibration, dissipation, and fluctuation processes are investigated in heavy-ion collisions over a broad range of energies, and it is noticed that mass equilibration in the quasifission reactions is a relatively slow process [44,45]. The stochastic mean-field (SMF) approach is also capable of stimulating the multinucleon exchange in quasifission reactions [46–48]. The dinuclear system (DNS) model is successfully developed to calculate the characteristics of charge, mass, and kinetic energy distributions of quasifission products [49–53].

The quasifission process is a significant reaction mechanism in multinucleon transfer reaction, which is favorable to produce the nuclei far from the entrance channel with many nucleons transferred. During the past decades, multinucleon transfer reactions have made great progress experimentally [54–61], and several unknown isotopes have been produced successfully [62–64]. It is found that multinucleon transfer reactions have the advantages to produce the nuclei near the  $N = 126$  shell [65–70] and the potential to produce the neutron-rich nuclei in the superheavy mass region [71–73]. For a comprehensive review, the Refs. [74–78] are recommended.

In the present paper, the contribution of the quasifission yields in the multinucleon transfer reaction  $^{136}\text{Xe} + ^{208}\text{Pb}$  is investigated. The paper is organized as follows. In Sec. II, the DNS model is introduced briefly. The calculated results and discussion are presented in Sec. III. Finally, the main conclusion is given in Sec. IV.

## II. MODEL

Within the framework of DNS model, the distribution probability of the fragment with proton number  $Z_1$  and neutron number  $N_1$  at time  $t$  is described by the master equation [79–81]:

$$\begin{aligned} \frac{dP(Z_1, N_1, t)}{dt} = & \sum_{Z'_1} W_{Z_1, N_1; Z'_1, N_1}(t) [d_{Z_1, N_1} P(Z'_1, N_1, t) \\ & - d_{Z'_1, N_1} P(Z_1, N_1, t)] \\ & + \sum_{N'_1} W_{Z_1, N_1; Z_1, N'_1}(t) [d_{Z_1, N_1} P(Z_1, N'_1, t) \\ & - d_{Z_1, N'_1} P(Z_1, N_1, t)] - [\Lambda_{\text{qf}}(\Theta(t)) \\ & + \Lambda_{\text{fis}}(\Theta(t))] P(Z_1, N_1, t). \end{aligned} \quad (1)$$

Here,  $W_{Z_1, N_1; Z'_1, N_1}$  ( $W_{Z_1, N_1; Z_1, N'_1}$ ) denotes the mean transition probability from channel  $(Z_1, N_1)$  to  $(Z'_1, N_1)$  [or from  $(Z_1, N_1)$  to  $(Z_1, N'_1)$ ].  $d_{Z_1, N_1}$  indicates the microscopic dimension associated with the macroscopic state  $(Z_1, N_1)$ . In our model, only one nucleon transfer process is considered during the dissipative collisions. The sum is taken over all possible proton and neutron numbers that the fragment  $(Z'_1, N_1')$  may have. The quasifission and fission rates in the DNS are denoted by  $\Lambda_{\text{qf}}$

and  $\Lambda_{\text{fis}}$ , respectively, calculated by one-dimensional Kramers equation [50].

The transition probability for proton transition is determined by the expression [79]:

$$\begin{aligned} W_{Z_1, N_1; Z'_1, N_1}(t) = & \frac{\tau_{\text{mem}}[Z_1, N_1, \epsilon_{\text{DNS}}^*(Z_1, N_1); Z'_1, N_1, \epsilon_{\text{DNS}}^*(Z'_1, N_1)]}{d_{Z_1, N_1} d_{Z'_1, N_1} \hbar^2} \\ & \sum_{ii'} |\langle Z'_1, N_1, \epsilon_{\text{DNS}}^*(Z'_1, N_1), i' | V(t) | \\ & Z_1, N_1, \epsilon_{\text{DNS}}^*(Z_1, N_1), i \rangle|^2. \end{aligned} \quad (2)$$

Here,  $\epsilon_{\text{DNS}}^*$  is the local excitation energy of DNS.  $i$  represents the remaining quantum number. The detailed descriptions of memory time  $\tau_{\text{mem}}$ ,  $V(t)$  and microscopic dimension  $d_{Z_1, N_1}$  can be found in Ref. [79]. The transition probability for neutron transition resembles the case for proton transition.

The local excitation energy of the DNS is displayed by the following formula:

$$\begin{aligned} \epsilon_{\text{DNS}}^* = & E_{\text{diss}} - [U(Z_1, N_1, Z_2, N_2) - U(Z_p, N_p, Z_t, N_t)] \\ & - \frac{(J - M)^2}{2\zeta_{\text{rel}}} - \frac{M^2}{2\zeta_{\text{int}}}, \end{aligned} \quad (3)$$

where  $E_{\text{diss}}$  denotes the energy dissipating from the relative kinetic energy into the composite system.  $U(Z_1, N_1, Z_2, N_2)$  represents the driving potential between the fragment  $(Z_1, N_1)$  and  $(Z_2, N_2)$ , and  $U(Z_p, N_p, Z_t, N_t)$  is that value in the entrance channel.  $\zeta_{\text{rel}}$  and  $\zeta_{\text{int}}$  indicate relative and intrinsic moments of inertia of the DNS, respectively.  $\zeta_{\text{rel}}$  is calculated by  $\zeta_{\text{rel}} = \mu R_{\text{cont}}^2$ .  $R_{\text{cont}}$  is the location where nucleon transfer takes place and estimated by:  $R_{\text{cont}} = R_1[1 + \beta_1 Y_{20}(\theta_1)] + R_2[1 + \beta_2 Y_{20}(\theta_2)] + 0.7 \text{ fm}$ . Here,  $R_{1,2} = 1.16 A_{1,2}^{1/3}$ .  $\beta_1$  and  $\beta_2$  are the quadrupole deformation parameters, originating from Ref. [82].  $\zeta_{\text{int}}$  is the sum of the intrinsic angular momenta of two fragments.  $J$  means the initial incident angular momentum and  $M$  is the intrinsic angular momentum from the dissipation of the relative angular momentum, which is calculated as  $M = J \cdot \zeta_{\text{int}} / (\zeta_{\text{int}} + \zeta_{\text{rel}})[1 - \exp(-t/\tau_J)]$ . Here,  $\tau_J$  is the angular momentum relaxation time and we set  $\tau_J = 12 \times 10^{-22} \text{ s}$ .

The energy dissipating from the incident energy into the DNS is shown as:

$$\begin{aligned} E_{\text{diss}}(t) = & E_{\text{c.m.}} - V_{\text{CN}}(Z_p, N_p, R_{\text{cont}}) \\ & - \frac{\langle J(t) \rangle^2}{2\zeta_{\text{rel}}} - E_{\text{rad}}(t). \end{aligned} \quad (4)$$

Here,  $V_{\text{CN}}(Z_p, N_p, R_{\text{cont}})$  is the interaction potential in the entrance channel. The mean relative angular momentum of the composite system is function of the evolution time and is described by  $\langle J(t) \rangle = J_{\text{st}} + (J - J_{\text{st}})\exp(-t/\tau_J)$ . The angular momentum at the sticking limit is  $J_{\text{st}} = J\zeta_{\text{rel}}/\zeta_{\text{tot}}$ . The radial kinetic energy  $E_{\text{rad}}(t) = E_{\text{rad}}(t=0)\exp(-t/\tau_R)$ , where  $\tau_R$  is the relaxation time of the radial kinetic energy and taken as the value  $\tau_R = 2 \times 10^{-22} \text{ s}$ . The initial radial energy is determined by  $E_{\text{rad}}(t=0) = E_{\text{c.m.}} - V_{\text{CN}}(Z_p, N_p, R_{\text{cont}}) - J^2/(2\zeta_{\text{rel}})$ .

The potential energy surface (PES) [22,50] is essential to drive the diffusion process and is expressed as:

$$U(Z_1, N_1, Z_2, N_2, R_{\text{cont}}) = \Delta(Z_1, N_1) + \Delta(Z_2, N_2) + V_{\text{CN}}(Z_1, N_1, Z_2, N_2, R_{\text{cont}}), \quad (5)$$

where  $\Delta(Z_1, N_1)$  and  $\Delta(Z_2, N_2)$  indicate the mass excesses of the both fragments.  $\Delta(Z, N)$  is estimated as:

$$\begin{aligned} \Delta(Z, N) = & Z\Delta_p + N\Delta_n - a_v(1 - \kappa I^2)A \\ & + a_s(1 - \kappa I^2)A^{2/3} + a_c Z^2/A^{1/3} - c_4 Z^2/A \\ & + E_{\text{pair}}(Z, N) + E_{\text{shell}}(Z, N). \end{aligned} \quad (6)$$

Here, the liquid drop parameters are  $a_v = 15.677 \text{ MeV}$ ,  $a_s = 18.56 \text{ MeV}$ ,  $a_c = 0.717 \text{ MeV}$ ,  $\kappa = 1.79$ , and  $c_4 = 1.211 \text{ MeV}$ .  $I = (N - Z)/A$  is the neutron-proton asymmetry. The pairing energy  $E_{\text{pair}}$  and shell correction energy  $E_{\text{shell}}$  are also included, and the details can be found in Ref. [82].

The production cross sections of the primary products formed in transfer processes are calculated as follows:

$$\begin{aligned} \sigma_{\text{pr}}(Z_1, N_1) = & \frac{\pi \hbar^2}{2\mu E_{\text{c.m.}}} \sum_J (2J + 1) \\ & \times [P(Z_1, N_1, t = \tau_{\text{int}}) + Y_{Z_1, N_1}]. \end{aligned}$$

Here,  $\mu$  is the reduced mass of the system and  $E_{\text{c.m.}}$  is the incident energy in the center of mass frame.  $P$  is the fragment distribution probability and  $\tau_{\text{int}}$  is the interaction time, determined by the deflection function method [83].  $Y_{Z_1, N_1}$  denotes the yield of the primary fragment  $(Z_1, N_1)$  from the quasifission process, which is obtained by [50]:

$$Y_{Z_1, N_1} = \int_0^{\tau_{\text{int}}} \Lambda_{Z_1, N_1}^{\text{qf}} P(Z_1, N_1, t) dt. \quad (7)$$

In the present work, the deexcitation processes of the excited fragments are treated with the GEMINI++ code [84,85]. GEMINI++ code is an improved version of the GEMINI sequential decay code [86,87], which can treat light particle evaporation, symmetric fission, and all possible binary-decay modes. The Hauser-Feshbach formalism is applied to simulate the evaporation of nucleons and light particles. The Moretto formalism is used to predict the emission of heavier fragments and asymmetric fission of a heavy system, while more symmetric fission of a heavy system is described by the Bohr-Wheeler formalism including the structure evolution.

### III. RESULTS AND DISCUSSION

#### A. Role of quasifission yields

The mass distribution with and without the quasifission yields in the reaction  ${}^{136}\text{Xe} + {}^{208}\text{Pb}$  at  $E_{\text{c.m.}} = 526 \text{ MeV}$  is shown in Fig. 1. As can be seen, the form probability including and excluding quasifission yields shows an opposite trend with increasing evolution time. The interaction time in  ${}^{136}\text{Xe} + {}^{208}\text{Pb}$  reaction at orbital angular momentum  $J = 10 \hbar$  is  $144 \times 10^{-22} \text{ s}$ , thus we select the evolution times  $t = 20 \times 10^{-22} \text{ s}$ ,  $50 \times 10^{-22} \text{ s}$ ,  $100 \times 10^{-22} \text{ s}$ , and  $140 \times 10^{-22} \text{ s}$  to investigate the dynamic process throughout the interaction time in Fig. 1(a). One can notice that the mass distribution

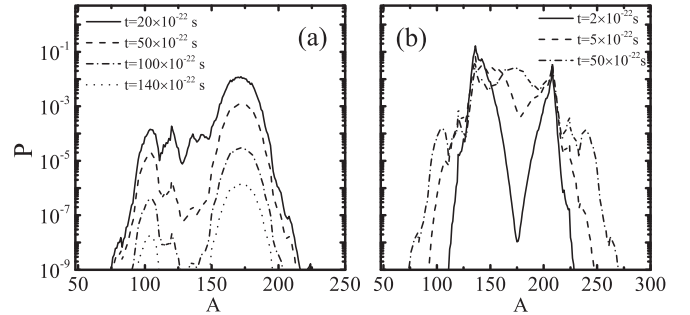


FIG. 1. (a) The mass distribution in the reaction  ${}^{136}\text{Xe} + {}^{208}\text{Pb}$  without the quasifission yields at  $E_{\text{c.m.}} = 526 \text{ MeV}$  with evolution time  $t = 20 \times 10^{-22} \text{ s}$  (solid line),  $t = 50 \times 10^{-22} \text{ s}$  (dashed line),  $t = 100 \times 10^{-22} \text{ s}$  (dash-dotted line), and  $t = 140 \times 10^{-22} \text{ s}$  (dotted line). (b) The mass distribution in  ${}^{136}\text{Xe} + {}^{208}\text{Pb}$  including the quasifission yields with evolution time  $t = 2 \times 10^{-22} \text{ s}$  (solid line),  $t = 5 \times 10^{-22} \text{ s}$  (dashed line), and  $t = 50 \times 10^{-22} \text{ s}$  (dash-dotted line).

becomes narrower with increasing evolution time. At  $t = 140 \times 10^{-22} \text{ s}$ , the two peaks locate around  $A = 100$  and  $A = 170$ , not the position near the projectile or target. What is more, one can find that the probability of all the fragments is not conserved. It becomes lower at a larger evolution time.

Figure 1(b) displays the results considering the contribution of quasifission yields. The mass equilibration is reached at around  $50 \times 10^{-22} \text{ s}$ , which is rather close to the timescale in Ref. [88]. Therefore, the evolution times  $t = 2 \times 10^{-22} \text{ s}$ ,  $5 \times 10^{-22} \text{ s}$ , and  $50 \times 10^{-22} \text{ s}$  are chosen within the timescale for mass equilibration. At the initial moment, the fragments distribute near the entrance channel. With increasing evolution time, the mass distribution becomes wider, which is consistent with common sense, because more nucleons can be transferred between the projectile and target at larger evolution time generally.

In Ref. [44], the timescale for full mass equilibration is around  $2 \times 10^{-20} \text{ s}$  by time-dependent Hartree-Fock approach, which is comparable to that in our calculations. TDHF is a fully microscopic model, which describes the dynamic process from the perspective of mean field formed by nucleon-nucleon interaction, taken as the Skyrme force. However, DNS is a semiclassical method and nucleon transfer process is governed by the potential energy surface. The great differences between these two models perhaps result in the discrepancy of mass equilibration time.

The incident angular momentum plays a vital role in the mass distribution. Figure 2 displays the production cross sections at different incident angular momenta. It can be seen the difference between including and excluding quasifission yields is more obvious at a lower angular momentum, which implies more fragments undergo quasifission within the interaction time. At  $J = 200$ , the difference is negligible. In the case at  $J = 10$  without quasifission yields, the mass distribution is the narrowest, and fragments with  $A = 110$ – $150$  and  $A = 200$ – $230$  are not produced, which is not consistent with the normal case. In general, the mass distributions are wider at a lower angular momentum and you can find that the

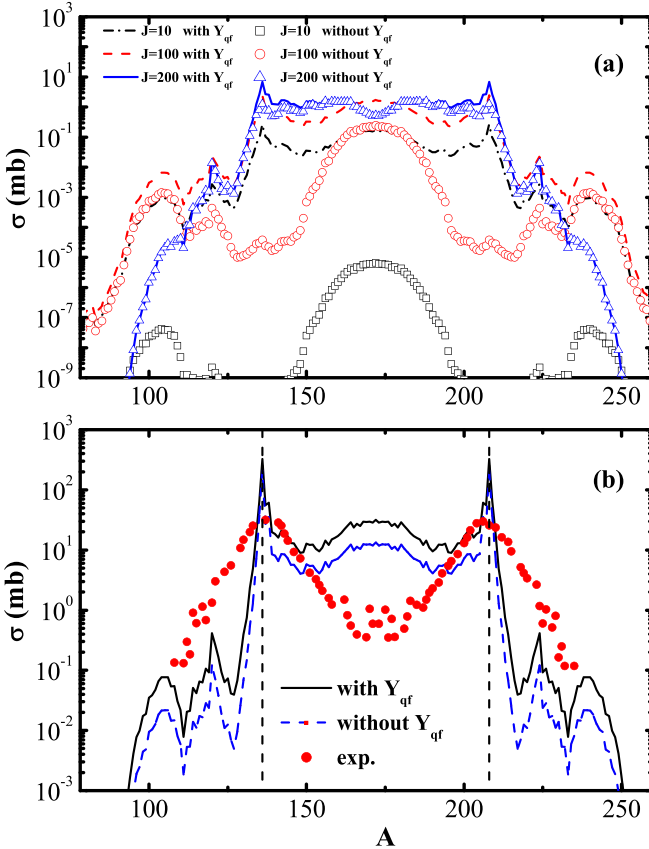


FIG. 2. (a) The mass distribution in  $^{136}\text{Xe} + ^{208}\text{Pb}$  reaction. The dash-dotted, dashed, and solid lines represent the cross sections including quasifission yields at quantum number of angular momentum  $J = 10$ ,  $J = 100$ , and  $J = 200$ , respectively. The blank square, circle, and triangle symbols denote the cross sections without quasifission yields at  $J = 10$ ,  $J = 100$ , and  $J = 200$ , respectively. (b) The comparison between the calculated mass distribution and experimental data. The solid and dashed lines display the results with and without quasifission yields, respectively. The experimental data are taken from Ref. [89].

distribution with quasifission yields becomes much wider at  $J = 10$ . Considering the quasifission yields, the peak value

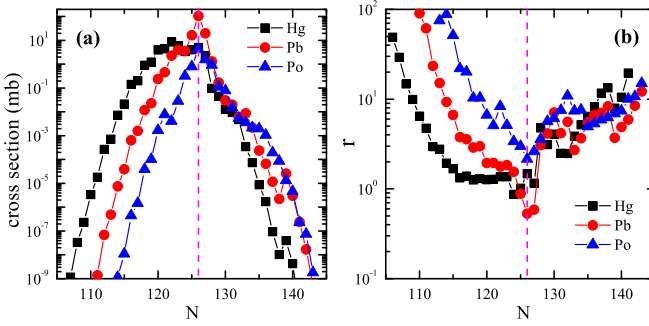


FIG. 3. (a) The primary production cross sections of Hg, Pb, and Po isotopes contributed from quasifission yields. (b) The ratios of Hg, Pb, and Po isotopes. The full square, circle, and triangle symbols denote the cases of Hg, Pb, and Po isotopes, respectively. The dash line present the position with  $N = 126$ .

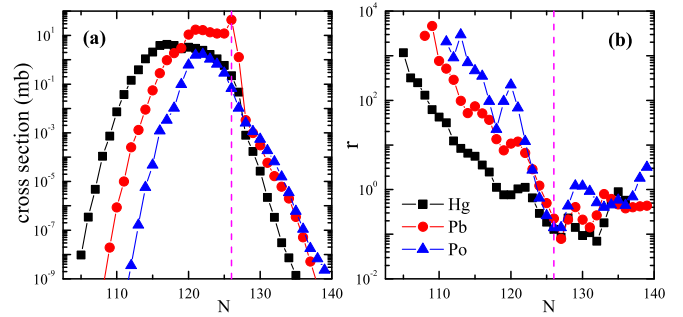


FIG. 4. (a) The final production cross sections of Hg, Pb, and Po isotopes contributed from quasifission yields. (b) The ratios of Hg, Pb, and Po isotopes. The full square, circle, and triangle symbols denote the cases of Hg, Pb, and Po isotopes, respectively. The dash line present the position with  $N = 126$ .

grows larger with increasing angular momentum, but the width of mass distribution shows an opposite trend. The comparison of the calculated mass distribution with the experimental data is shown in Fig. 2(b). The production cross sections are the sum of all the partial-wave cross sections. Due to the supplement of quasifission yields, the production cross sections are enhanced for all the fragments. Although the cross sections of the intermediate-mass fragments are overestimated, the cross sections including quasifission yields are in a better agreement with the experimental data in the region of the mass smaller than the projectile and larger than the target.

The contribution from the quasifission yields to the production cross sections can be extracted. The primary production cross sections of Hg, Pb, and Po isotopes contributed from quasifission yields are shown in Fig. 3(a). It can be seen that the cross sections from quasifission yields are higher in the region near the target and become lower with more neutrons transferred. To weigh the impact of quasifission, it is reasonable to use relative sizes as the criterion. The ratio  $r$  is defined as  $r = \sigma_{\text{qf}}/\sigma_{\text{noqf}}$ , where  $\sigma_{\text{qf}}$  represents the production cross sections contributed from quasifission yields, and  $\sigma_{\text{noqf}}$  denotes the cross sections without quasifission yields. From Fig. 3(b), one can see that the ratios near the target are lower, implying that the impact on the primary production cross sections is smaller. On the neutron-rich side, the ratios are

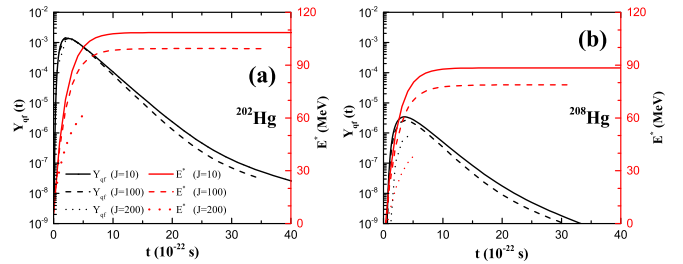


FIG. 5. The quasifission yield and excitation energy of the isotopes (a)  $^{202}\text{Hg}$  and (b)  $^{208}\text{Hg}$  as a function of evolution time. The solid line, dashed and dotted lines denote the results at  $J = 10$ ,  $J = 100$ , and  $J = 200$ , respectively.

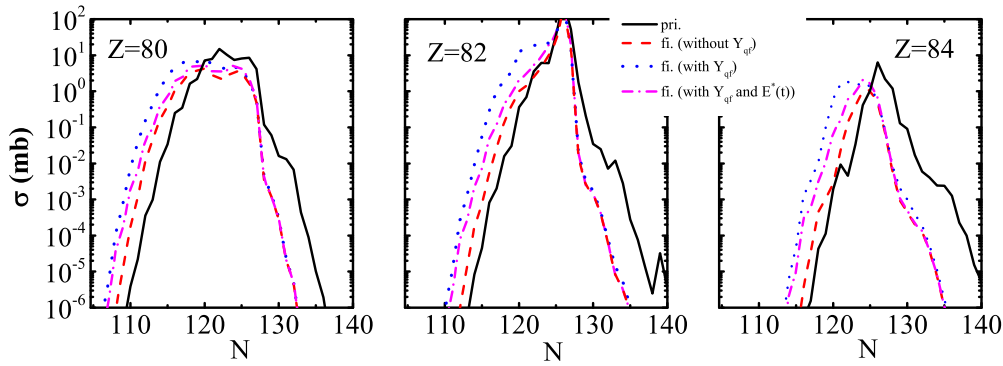


FIG. 6. The isotopic distribution of isotopes with  $Z = 80$  (Hg),  $Z = 82$  (Pb), and  $Z = 84$  (Po), respectively. The solid line denotes the production cross sections of the primary fragments, while the dashed line denotes the cross sections of the final fragments without quasifission yields. The dotted line represents the final production cross sections considering quasifission yields but with the excitation energy taken at interaction time. The dash-dotted line shows the results considering the quasifission yields and time-dependent excitation energy.

in the range of 1–10. However, the ratios increase rapidly with more neutrons transferred, especially for Pb and Hg isotopes. Therefore, the impact on the primary cross sections of neutron-deficient isotopes is remarkable.

Experimentally, more attention is paid to the impact from the quasifission yields on the final production cross sections. The final production cross sections of Hg, Pb, and Po isotopes contributed from quasifission yields are shown in Fig. 4(a). The trends are similar to the case of primary cross section in Fig. 3. The cross sections from quasifission yields are larger near the target, but the corresponding ratios are lower. The impact on the final cross sections of the neutron-deficient isotopes is larger because the ratios of neutron-deficient isotopes are much higher than neutron-rich nuclei. The ratios of neutron-rich isotopes concentrate on the range of 0.1–1, which are much lower than those of the primary neutron-rich nuclei, and the cross sections of neutron-rich nuclei achieve a onefold increase at most. Therefore, the impact of the quasifission yields on the neutron-deficient isotopes is greater than the neutron-rich isotopes.

### B. Deexcite the quasifission fragments

Indeed, the excitation energy of the fragments by quasifission within interaction time is a function of evolution time. Figure 5 shows the quasifission yield and excitation energy of the isotopes  $^{202,208}\text{Hg}$  as a function of evolution time. One can see that the excitation energy increases rapidly at the initial stage and reaches a stable value at evolution time larger than  $10 \times 10^{-22}$  s. The excitation energy of the fragment is larger with a lower angular momentum because rotation energy of the dinuclear system is lower in that case, leading to a higher excitation energy. For a simple addition to the final cross section from quasifission yields, the excitation energy is taken as the value at interaction time. However, the quasifission yields increase sharply at the initial stage, concentrating on the evolution time from about  $2 \times 10^{-22}$  s to  $10 \times 10^{-22}$  s. Therefore, most of the quasifission fragments have lower excitation energy comparing with the value at the interaction time. For a better description of the final cross sections, it

is reasonable to deexcite the quasifission fragments in every moment. Comparing the results of these two nuclei, one can find the excitation energy of  $^{202}\text{Hg}$  is about 20 MeV higher than that for the neutron-rich isotope  $^{208}\text{Hg}$  at the identical angular momentum. The quasifission yields of  $^{202}\text{Hg}$  are also much larger than those for  $^{208}\text{Hg}$ .

The isotopic distribution of isotopes with  $Z = 80$ ,  $Z = 82$ , and  $Z = 84$  is presented in Fig. 6. The dashed lines denote the final production cross sections without the quasifission yields, the dotted lines represent the case considering quasifission yields but with the excitation energy taken at interaction time, and the dash-dotted lines show the situation including quasifission yields and time-dependent excitation energy. For convenient description, we name the above three cases as case 1, case 2, and case 3. It is clear that the cross sections without quasifission yields are the lowest. In case 2, primary fragments tend to evaporate more neutrons, because the excitation energy at the interaction time is higher. However, in case 3, the excitation energy changes over evolution time and is lower than the excitation energy at the interaction time. Therefore, fewer neutrons are evaporated in case 3 compared with case 2. What is more, the differences in those three cases are more obvious on the neutron-deficient side. On the neutron-rich side, the cross sections stay almost invariable. That behavior can be interpreted according to Fig. 5. It can be found that the quasifission yields for the neutron-rich nuclei are much lower. In addition, the excited quasifission fragments tend to evaporate neutrons, which is favorable to enhance the production cross sections of neutron-deficient isotopes.

### IV. CONCLUSIONS

The mass distribution in  $^{136}\text{Xe} + ^{208}\text{Pb}$  is investigated within the DNS model. By adding the contribution of quasifission yields, the probability of all the fragments is conserved, and the mass distribution becomes wider with increasing the evolution time. The influence of the incident angular momentum on the mass distribution and isotopic distribution is also studied. It is found the difference between including and excluding quasifission yields is more significant at

lower angular momentum. Comparing the calculated mass distribution with the experimental one, the cross sections with the quasifission yields are in a better agreement with the experimental data in the region of the mass smaller than the projectile and larger than the target, although the yields of the intermediate-mass fragments are overpredicted. The final cross sections of neutron-rich nuclei achieve a onefold increase at most adding the quasifission yields. The impact from the quasifission yields on the neutron-deficient isotopes is greater than the neutron-rich isotopes.

The excitation energy and quasifission yield of the fragments is a function of evolution time. The quasifission yields concentrate on the initial stage of evolution time, corresponding to lower excitation energy. Thus, the fragments formed by quasifission yields should be deexcited in every moment. The production cross sections of the final fragments in the following three cases are compared, excluding quasifission yields, including quasifission yields with time-dependent

excitation energy, and including quasifission yields with the excitation energy at the interaction time. The cross sections without quasifission yields are the lowest. Due to the lower excitation energy in the case with time-dependent excitation energy, fewer neutrons are evaporated comparing to the case with the excitation energy at the interaction time.

## ACKNOWLEDGMENTS

We thank Dr. Peiwei Wen for the valuable comments to improve the manuscript. This work was supported by the National Natural Science Foundation of China under Grants No. 11635003, No. 11961141004, No. 11025524, and No. 11161130520; the National Basic Research Program of China under Grant No. 2010CB832903; the European Commissions 7th Framework Programme (Fp7-PEOPLE-2010-IRSES) under Grant No. 269131.

- 
- [1] B. Heusch, C. Volant, H. Freiesleben, R. P. Chestnut, K. D. Hildenbrand, F. Pühlhofer, and W. F. W. Schneider, *Z. Phys. A* **288**, 391 (1978).
  - [2] B. B. Back, R. R. Betts, K. Cassidy, B. G. Glagola, J. E. Gindler, L. E. Glendenin, and B. D. Wilkins, *Phys. Rev. Lett.* **50**, 818 (1983).
  - [3] G. Rudolf, A. Gobbi, H. Stelzer, U. Lynen, A. Olmi, H. Sann, R. G. Stokstad, and D. Pelte, *Nucl. Phys. A* **330**, 243 (1979).
  - [4] L. G. Moretto, *Nucl. Phys. A* **409**, 115 (1983).
  - [5] J. Töke, R. Bock, G. X. Dai, A. Gobbi, S. Gralla, K. D. Hildenbrand, J. Kuzminski, W. F. J. Müller, A. Olmi, H. Stelzer, B. B. Back, and S. Bjørnholm, *Nucl. Phys. A* **440**, 327 (1985).
  - [6] R. Bock, Y. T. Chu, M. Dakowski, A. Gobbi, E. Grosse, A. Olmi, H. Sann, D. Schwalm, L. Lynen, W. Müller, S. Bjørnholm, H. Esbensen, W. Wölfli, and E. Morenzoni, *Nucl. Phys. A* **388**, 334 (1982).
  - [7] C. Lebrun, F. Hanappe, J. F. LeColley, F. Lefebvres, C. Ngô, J. Péter, and B. Tamain, *Nucl. Phys. A* **321**, 207 (1979).
  - [8] B. Borderie, M. Berlanger, D. Gardès, F. Hanappe, L. Nowicki, J. Péter, B. Tamain, S. Agarwal, J. Girard, C. Grégoire, J. Matuszek, and C. Ngô, *Z. Phys. A* **299**, 263 (1981).
  - [9] M. B. Tsang, H. Utsunomiya, C. K. Gelbke, W. G. Lynch, B. B. Back, S. Saini, P. A. Baisden, and M. A. McMahan, *Phys. Lett. B* **129**, 18 (1983).
  - [10] M. B. Tsang, D. Ardouin, C. K. Gelbke, W. G. Lynch, Z. R. Xu, B. B. Back, R. Betts, S. Saini, P. A. Baisden, and M. A. McMahan, *Phys. Rev. C* **28**, 747 (1983).
  - [11] W. Q. Shen, J. Albinski, A. Gobbi, S. Gralla, K. D. Hildenbrand, N. Herrmann, J. Kuzminski, W. F. J. Müller, H. Stelzer, J. Töke, B. B. Back, S. Bjørnholm, and S. P. Sørensen, *Phys. Rev. C* **36**, 115 (1987).
  - [12] S. A. Kalandarov, G. G. Adamian, N. V. Antonenko, and W. Scheid, *Phys. Rev. C* **83**, 054611 (2011).
  - [13] B. B. Back, S. Bjørnholm, T. Døssing, W. Q. Shen, K. D. Hildenbrand, A. Gobbi, and S. P. Sørensen, *Phys. Rev. C* **41**, 1495 (1990).
  - [14] T. K. Ghosh, K. Banerjee, C. Bhattacharya, S. Bhattacharya, S. Kundu, P. Mali, J. K. Meena, G. Mukherjee, S. Mukhopadhyay, T. K. Rana, P. Bhattacharya, and K. S. Golda, *Phys. Rev. C* **79**, 054607 (2009).
  - [15] I. M. Itkis, E. M. Kozulin, M. G. Itkis, G. N. Knyazheva, A. A. Bogachev, E. V. Chernysheva, L. Krupa, Yu. Ts. Oganessian, V. I. Zagrebaev, A. Ya. Rusanov, F. Goennenwein, O. Dorvaux, L. Stuttgé, F. Hanappe, E. Vardaci, and E. de Goés Brennand, *Phys. Rev. C* **83**, 064613 (2011).
  - [16] G. Mohanto, D. J. Hinde, K. Banerjee, M. Dasgupta, D. Y. Jeung, C. Simenel, E. C. Simpson, A. Wakhle, E. Williams, I. P. Carter, K. J. Cook, D. H. Luong, C. S. Palshetkar, and D. C. Rafferty, *Phys. Rev. C* **97**, 054603 (2018).
  - [17] R. Rafiei, R. G. Thomas, D. J. Hinde, M. Dasgupta, C. R. Morton, L. R. Gasques, M. L. Brown, and M. D. Rodriguez, *Phys. Rev. C* **77**, 024606 (2008).
  - [18] C. Yadav, R. G. Thomas, R. K. Choudhury, P. Sugathan, A. Jhingan, S. Appannababu, K. S. Golda, D. Singh, Ish Mukul, J. Gehlot, E. Prasad, and H. J. Wollersheim, *Phys. Rev. C* **86**, 034606 (2012).
  - [19] B. B. Back, *Phys. Rev. C* **31**, 2104 (1985).
  - [20] D. J. Hinde, M. Dasgupta, J. R. Leigh, J. P. Lestone, J. C. Mein, C. R. Morton, J. O. Newton, and H. Timmers, *Phys. Rev. Lett.* **74**, 1295 (1995).
  - [21] D. J. Hinde, M. Dasgupta, J. R. Leigh, J. C. Mein, C. R. Morton, J. O. Newton, and H. Timmers, *Phys. Rev. C* **53**, 1290 (1996).
  - [22] G. G. Adamian, N. V. Antonenko, and W. Scheid, *Nucl. Phys. A* **618**, 176 (1997).
  - [23] A. Diaz-Torres, G. G. Adamian, N. V. Antonenko, and W. Scheid, *Phys. Rev. C* **64**, 024604 (2001).
  - [24] D. J. Hinde, M. Dasgupta, and A. Mukherjee, *Phys. Rev. Lett.* **89**, 282701 (2002).
  - [25] V. A. Rubchenya, W. H. Trzaska, and E. Vardaci, *Int. J. Mod. Phys. E* **18**, 830 (2009).
  - [26] G. G. Adamian, N. V. Antonenko, and A. S. Zubov, *Phys. Rev. C* **71**, 034603 (2005).
  - [27] D. J. Kedziora and C. Simenel, *Phys. Rev. C* **81**, 044613 (2010).
  - [28] E. M. Kozulin, V. I. Zagrebaev, G. N. Knyazheva, I. M. Itkis, K. V. Novikov, M. G. Itkis, S. N. Dmitriev, I. M. Harca, A. E. Bondarchenko, A. V. Karpov, V. V. Saiko, and E. Vardaci, *Phys. Rev. C* **96**, 064621 (2017).

- [29] A. K. Nasirov, A. I. Muminov, R. K. Utamuratov, G. Fazio, G. Giardina, F. Hanappe, G. Mandaglio, M. Manganaro, and W. Scheid, *Eur. Phys. J. A* **34**, 325 (2007).
- [30] A. K. Nasirov, G. Giardina, G. Mandaglio, M. Manganaro, F. Hanappe, S. Heinz, S. Hofmann, A. I. Muminov, and W. Scheid, *Phys. Rev. C* **79**, 024606 (2009).
- [31] H. Q. Zhang, C. L. Zhang, C. J. Lin, Z. H. Liu, F. Yang, A. K. Nasirov, G. Mandaglio, M. Manganaro, and G. Giardina, *Phys. Rev. C* **81**, 034611 (2010).
- [32] C. Simenel, D. J. Hinde, R. du Rietz, M. Dasgupta, M. Evers, C. J. Lin, D. H. Luong, and A. Wakhle, *Phys. Lett. B* **710**, 607 (2012).
- [33] K. Sekizawa and K. Yabana, *Phys. Rev. C* **88**, 014614 (2013).
- [34] A. Wakhle, C. Simenel, D. J. Hinde, M. Dasgupta, M. Evers, D. H. Luong, R. du Rietz, and E. Williams, *Phys. Rev. Lett.* **113**, 182502 (2014).
- [35] V. E. Oberacker, A. S. Umar, and C. Simenel, *Phys. Rev. C* **90**, 054605 (2014).
- [36] A. S. Umar, V. E. Oberacker, and C. Simenel, *Phys. Rev. C* **92**, 024621 (2015).
- [37] S. Ayik, B. Yilmaz, and O. Yilmaz, *Phys. Rev. C* **92**, 064615 (2015).
- [38] K. Sekizawa and K. Yabana, *Phys. Rev. C* **93**, 054616 (2016).
- [39] K. Sekizawa, *Phys. Rev. C* **96**, 014615 (2017).
- [40] K. Sekizawa, *Phys. Rev. C* **96**, 014601(R) (2017).
- [41] C. Simenel and A. S. Umar, *Prog. Part. Nucl. Phys.* **103**, 19 (2018).
- [42] K. Sekizawa, *Front. Phys.* **7**, 20 (2019).
- [43] K. Godbey, C. Simenel, and A. S. Umar, *Phys. Rev. C* **101**, 034602 (2020).
- [44] C. Simenel, K. Godbey, and A. S. Umar, *Phys. Rev. Lett.* **124**, 212504 (2020).
- [45] A. S. Umar, V. E. Oberacker, and C. Simenel, *Phys. Rev. C* **94**, 024605 (2016).
- [46] S. Ayik, B. Yilmaz, O. Yilmaz, and A. S. Umar, *Phys. Rev. C* **97**, 054618 (2018).
- [47] S. Ayik, B. Yilmaz, O. Yilmaz, and A. S. Umar, *Phys. Rev. C* **100**, 014609 (2019).
- [48] S. Ayik, O. Yilmaz, B. Yilmaz, and A. S. Umar, *Phys. Rev. C* **100**, 044614 (2019).
- [49] G. G. Adamian, N. V. Antonenko, W. Scheid, and V. V. Volkov, *Nucl. Phys. A* **627**, 361 (1997).
- [50] G. G. Adamian, N. V. Antonenko, and W. Scheid, *Phys. Rev. C* **68**, 034601 (2003).
- [51] A. K. Nasirov, G. Mandaglio, M. Manganaro, A. I. Muminov, G. Fazio, and G. Giardina, *Phys. Lett. B* **686**, 72 (2010).
- [52] A. Nasirov, K. Kim, G. Mandaglio, G. Giardina, A. Muminov, and Y. Kim, *Eur. Phys. J. A* **49**, 147 (2013).
- [53] A. Shamlath, E. Prasad, N. Madhavan, P. V. Laveen, J. Gehlot, A. K. Nasirov, G. Giardina, G. Mandaglio, S. Nath, T. Banerjee, A. M. Vinodkumar, M. Shareef, A. Jhingan, T. Varughese, DVGRKS Kumar, P. S. Devi, Khushboo, P. Jisha, N. Kumar, M. M. Hosamani, and S. Kailas, *Phys. Rev. C* **95**, 034610 (2017).
- [54] E. M. Kozulin, G. N. Knyazheva, S. N. Dmitriev, I. M. Itkis, M. G. Itkis, T. A. Loktev, K. V. Novikov, A. N. Baranov, W. H. Trzaska, E. Vardaci, S. Heinz, O. Beliuskina, and S. V. Khlebnikov, *Phys. Rev. C* **89**, 014614 (2014).
- [55] J. S. Barrett, W. Loveland, R. Yanez, S. Zhu, A. D. Ayangeakaa, M. P. Carpenter, J. P. Greene, R. V. F. Janssens, T. Lauritsen, E. A. McCutchan, A. A. Sonzogni, C. J. Chiara, J. L. Harker, and W. B. Walters, *Phys. Rev. C* **91**, 064615 (2015).
- [56] A. Vogt, B. Birkenbach, P. Reiter, L. Corradi, T. Mijatović, D. Montanari, S. Szilner, D. Bazzacco, M. Bowry, A. Bracco, B. Bruyneel, F. C. L. Crespi, G. de Angelis, P. Désesquelles, J. Eberth, E. Farnea, E. Fioretto, A. Gadea, K. Geibel, A. Gengelbach, A. Giaz, A. Görgen, A. Gottardo, J. Grebosz, H. Hess, P. R. John, J. Jolie, D. S. Judson, A. Jungclaus, W. Korten, S. Leoni, S. Lunardi, R. Menegazzo, D. Mengoni, C. Michelagnoli, G. Montagnoli, D. Napoli, L. Pellegrini, G. Pollarolo, A. Pullia, B. Quintana, F. Radeck, F. Recchia, D. Rosso, E. Şahin, M. D. Salsac, F. Scarlassara, P.-A. Söderström, A. M. Stefanini, T. Steinbach, O. Stezowski, B. Szpak, C. Theisen, C. Ur, J. J. Valiente-Dobón, V. Vandone, and A. Wiens, *Phys. Rev. C* **92**, 024619 (2015).
- [57] T. Welsh, W. Loveland, R. Yanez, J. S. Barrett, E. A. McCutchan, A. A. Sonzogni, T. Johnson, S. Zhu, J. P. Greene, A. D. Ayangeakaa, M. P. Carpenter, T. Lauritsen, J. L. Harker, W. B. Walters, B. M. S. Amro, and P. Copp, *Phys. Lett. B* **771**, 119 (2017).
- [58] F. Galtarossa, L. Corradi, S. Szilner, E. Fioretto, G. Pollarolo, T. Mijatović, D. Montanari, D. Ackermann, D. Bourgin, S. Courtin, G. Fruet, A. Goasduff, J. Grebosz, F. Haas, D. Jelavić Malenica, S. C. Jeong, H. M. Jia, P. R. John, D. Mengoni, M. Milin, G. Montagnoli, F. Scarlassara, N. Skukan, N. Soić, A. M. Stefanini, E. Strano, V. Tokić, C. A. Ur, J. J. Valiente-Dobón, and Y. X. Watanabe, *Phys. Rev. C* **97**, 054606 (2018).
- [59] V. V. Desai, W. Loveland, K. McCaleb, R. Yanez, G. Lane, S. S. Hota, M. W. Reed, H. Watanabe, S. Zhu, K. Auranden, A. D. Ayangeakaa, M. P. Carpenter, J. P. Greene, F. G. Kondev, D. Seweryniak, R. V. F. Janssens, and P. A. Copp, *Phys. Rev. C* **99**, 044604 (2019).
- [60] V. V. Desai, A. Pica, W. Loveland, and J. S. Barrett, E. A. McCutchan, S. Zhu, A. D. Ayangeakaa, M. P. Carpenter, J. P. Greene, T. Lauritsen, R. V. F. Janssens, B. M. S. Amro, and W. B. Walters, *Phys. Rev. C* **101**, 034612 (2020).
- [61] V. V. Desai, W. Loveland, R. Yanez, G. Lane, S. Zhu, A. D. Ayangeakaa, J. P. Greene, F. G. Kondev, R. V. F. Janssens, and P. A. Copp, *Eur. Phys. J. A* **56**, 150 (2020).
- [62] H. M. Devaraja, S. Heinz, O. Beliuskina, V. Comas, S. Hofmann, C. Hornung, G. Münzenberg, K. Nishio, D. Ackermann, Y. K. Gambhir, M. Gupta, R. A. Henderson, F. P. Heßberger, J. Khuyagbaatar, B. Kindler, B. Lommel, K. J. Moody, J. Maurer, R. Mann, A. G. Popeko, D. A. Shaughnessy, M. A. Stoyer, and A. V. Yeremin, *Phys. Lett. B* **748**, 199 (2015).
- [63] S. Heinz, H. M. Devaraja, O. Beliuskina, V. Comas, S. Hofmann, C. Hornung, G. Münzenberg, D. Ackermann, M. Gupta, R. A. Henderson, F. P. Heßberger, B. Kindler, B. Lommel, R. Mann, J. Maurer, K. J. Moody, K. Nishio, A. G. Popeko, D. A. Shaughnessy, M. A. Stoyer, and A. V. Yeremin, *Eur. Phys. J. A* **52**, 278 (2016).
- [64] H. M. Devaraja, S. Heinz, O. Beliuskina, S. Hofmann, C. Hornung, G. Münzenberg, D. Ackermann, M. Gupta, Y. K. Gambhir, R. A. Henderson, F. P. Heßberger, A. V. Yeremin, B. Kindler, B. Lommel, J. Maurer, K. J. Moody, K. Nishio, A. G. Popeko, M. A. Stoyer, and D. A. Shaughnessy, *Eur. Phys. J. A* **55**, 25 (2019).
- [65] V. Zagrebaev and W. Greiner, *J. Phys. G: Nucl. Part. Phys.* **35**, 125103 (2008).
- [66] V. Zagrebaev and W. Greiner, *Phys. Rev. Lett.* **101**, 122701 (2008).

- [67] V. F. Comas, S. Heinz, S. Hofmann, D. Ackermann, J. A. Heredia, F. P. Heßberger, J. Khuyagbaatar, B. Kindler, B. Lommel, and R. Mann, *Eur. Phys. J. A* **49**, 112 (2013).
- [68] O. Beliuskina, S. Heinz, V. Zagrebaev, V. Comas, C. Heinz, S. Hofmann, R. Knöbel, M. Stahl, D. Ackermann, F. P. Heßberger, B. Kindler, B. Lommel, J. Maurer, and R. Mann, *Eur. Phys. J. A* **50**, 161 (2014).
- [69] Y. X. Watanabe, Y. H. Kim, S. C. Jeong, Y. Hirayama, N. Imai, H. Ishiyama, H. S. Jung, H. Miyatake, S. Choi, J. S. Song, E. Clement, G. de France, A. Navin, M. Rejmund, C. Schmitt, G. Pollarolo, L. Corradi, E. Fioretto, D. Montanari, M. Niikura, D. Suzuki, H. Nishibata, and J. Takatsu, *Phys. Rev. Lett.* **115**, 172503 (2015).
- [70] K. Novikov, I. M. Harca, E. M. Kozulin, S. Dmitriev, J. Itkis, G. Knyazheva, T. Loktev, L. Corradi, J. Valiente-Dobon, E. Fioretto, D. Montanari, A. M. Stefanini, E. Vardaci, D. Quero, G. Montagnoli, F. Scarlassara, E. Strano, G. Pollarolo, J. Piot, T. Mijatovic, S. Szilner, D. Ackermann, G. Chubarian, and W. H. Trzaska, *J. Phys.: Conf. Ser.* **703**, 012020 (2016).
- [71] V. I. Zagrebaev, Yu. Ts. Oganessian, M. G. Itkis, and W. Greiner, *Phys. Rev. C* **73**, 031602(R) (2006).
- [72] V. I. Zagrebaev and W. Greiner, *Phys. Rev. C* **83**, 044618 (2011).
- [73] V. I. Zagrebaev and W. Greiner, *Phys. Rev. C* **87**, 034608 (2013).
- [74] L. Corradi, G. Pollarolo, and S. Szilner, *J. Phys. G: Nucl. Part. Phys.* **36**, 113101 (2009).
- [75] F. S. Zhang, C. Li, L. Zhu, and P. W. Wen, *Front. Phys.* **13**, 132113 (2018).
- [76] W. D. Loveland, *Front. Phys.* **7**, 23 (2019).
- [77] G. G. Adamian, N. V. Antonenko, A. Diaz-Torres, and S. Heinz, *Eur. Phys. J. A* **56**, 47 (2020).
- [78] L. Zhu, C. Li, C. C. Guo, J. Su, P. W. Wen, G. Zhang, and F. S. Zhang, *Int. J. Mod. Phys. E* **29**, 2030004 (2020).
- [79] S. Ayik, B. Schürmann, and W. Nörenberg, *Z. Phys. A* **277**, 299 (1976).
- [80] L. Zhu, F. S. Zhang, P. W. Wen, J. Su, and W. J. Xie, *Phys. Rev. C* **96**, 024606 (2017).
- [81] Z. Q. Feng, *Phys. Rev. C* **95**, 024615 (2017).
- [82] P. Möller, J. R. Nix, W. D. Myers, and W. J. Swiatecki, *At. Data Nucl. Data Tables* **59**, 185 (1995).
- [83] G. Wolschin and W. Nörenberg, *Z. Phys. A* **284**, 209 (1978).
- [84] R. J. Charity, *Phys. Rev. C* **82**, 014610 (2010).
- [85] D. Mancusi, R. J. Charity, and J. Cugnon, *Phys. Rev. C* **82**, 044610 (2010).
- [86] L. G. Moretto, *Nucl. Phys. A* **247**, 211 (1975).
- [87] R. J. Charity, M. A. McMahan, G. J. Wozniak, R. J. McDonald, L. G. Moretto, D. G. Sarantites, L. G. Sobotka, G. Guarino, A. Pantaleo, L. Fiore, A. Gobbi, and K. D. Hildenbrand, *Nucl. Phys. A* **483**, 371 (1988).
- [88] L. Zhu, Z. Q. Feng, and F. S. Zhang, *J. Phys. G: Nucl. Part. Phys.* **42**, 085102 (2015).
- [89] E. M. Kozulin, E. Vardaci, G. N. Knyazheva, A. A. Bogachev, S. N. Dmitriev, I. M. Itkis, M. G. Itkis, A. G. Knyazev, T. A. Loktev, K. V. Novikov, E. A. Razinkov, O. V. Rudakov, S. V. Smirnov, W. Trzaska, and V. I. Zagrebaev, *Phys. Rev. C* **86**, 044611 (2012).